Nanoscale Advances

ROYAL SOCIETY OF CHEMISTRY

PAPER

View Article Online
View Journal | View Issue

Open Access Article. Published on 10 August 2021. Downloaded on 11/12/2025 2:54:25 PM.
This article is licensed under a Creative Commons Attribution-NonCommercial 3.0 Unported Licence.

Check for updates

Cite this: *Nanoscale Adv.*, 2021, **3**, 5823

Grafting chelating groups on 2D carbon for selective heavy metal adsorption†

Risa Shibahara,[a] Kazuhide Kamiya[bcd] and Yuta Nishina*[ae]

Received 11th June 2021
Accepted 10th August 2021

DOI: 10.1039/d1na00435b

rsc.li/nanoscale-advances

Iminodiacetic acid (IDA) is a tridentate ligand, which can capture metal ions by forming two fused five-membered chelate rings. In this study, we fixed IDA moieties onto a two-dimensional nanocarbon, graphene oxide (GO), to obtain materials with high and selective adsorption of metal ions. The synthesis conditions for the GO–IDA composites were optimized, then their structures were characterized by infrared spectroscopy (FT-IR), X-ray photoelectron spectroscopy (XPS), and CHN elemental analysis. In addition, the heavy-metal removal efficiency and selectivity of the GO–IDA composites with different length alkyl linkers between the GO and IDA were investigated. An aqueous solution containing 10 metal ions (Al, As, B, Cd, Cr, Cu, Mn, Pb, Se, and Zn) was used as a model for contaminated water at pH 7, and the interactions of the ions with GO–IDA were in the order of Cu > Pb > As > B > Zn > Al ≈ Se. The interaction between Cu and GO–IDA was confirmed by XPS and extended X-ray absorption fine structure (EXAFS), which showed that Cu was coordinated to IDA.

1. Introduction

Due to the rapid development of industries including mining, electroplating, leather production, and metal plating, wastewater contains harmful heavy metals.[1,2] Unlike organic pollutants, heavy metals are not biodegradable and are likely to accumulate in the body.[3] Some heavy metals such as As, Cd, Cu, Hg, and Pb are toxic and/or carcinogenic, causing health problems. Heavy metals are naturally present in groundwater,[4,5] which has caused severe health problems for 6 million people all over the world.[6–11] Therefore, heavy-metal removal methods which are cheap, convenient, and easy for treating daily drinking water are critical. So far, heavy metals in water have been removed by ion exchange,[12] precipitation,[13] reverse osmosis,[14] electrochemical treatment,[15] and adsorption.[16] Among them, adsorption is especially useful because it is a simple and contamination-free process.[17–20] Iminodiacetic acid (IDA) shows excellent potential for adsorption of heavy metals (Table S1†);[21] therefore, IDA-immobilized resins are widely used both in analytical research and industry.[22,23] The metal ions on IDA can be desorbed by treating with an acid solution;[24] subsequent treatment with a basic solution enables the resins to be reused. However, pristine IDA is soluble in water, and recovery is the issue to be solved. In this study, we aimed to develop a solid-state, high-performance, and recyclable adsorbent for heavy metal ions. As a support material for IDA, we focused on graphene oxide (GO), a carbon material with a high specific surface area, good hydrophilicity and biosafety.[25–30] GO itself has been reported to have metal adsorption capacity, and GO-based composites have been reported to have high Pb and As removal efficiency.[31–37] These reports show the great potential of GO. However, testing GO materials for selective removal of metals is still not reported; the previous studies have focused on a specific metal species, which is far from actual contaminated water in the environment.[38] For more practical evaluation of the selective adsorption by GO–IDA composites, we used a solution containing 10 types of metal ions. The adsorption mechanism was investigated to provide guidance for excellent, selective, heavy-metal removal.

2. Results and discussion

2.1 Covalent functionalization of GO and structure analysis

Covalent functionalization of GO with amine through epoxy ring-opening amination was applied in this research.[39] We initially screened the reaction conditions for the amination of GO using simple alkylamine as a model compound, then applying the optimized conditions to our specific target molecule, IDA. The nitrogen content can be a good indicator for the amine functionalization, therefore, we employed elemental

[a]Graduate School of Natural Science & Technology, Okayama University, 3-1-1 Tsushimanaka, Kita-ku, Okayama 700-8530, Japan. E-mail: nisina-y@cc.okayama-u.ac.jp

[b]Graduate School of Engineering Science, Osaka University, 1-3 Machikaneyama, Toyonaka, Osaka, 560-8531, Japan

[c]Research Center for Solar Energy Chemistry, Osaka University, 1-3 Machikaneyama, Toyonaka, Osaka 560-8531, Japan

[d]Innovative Catalysis Science Division, Institute for Open and Transdisciplinary Research Initiatives (ICS-OTRI), Osaka University, Suita, Osaka 565-0871, Japan

[e]Research Core for Interdisciplinary Science, Okayama University, 3-1-1 Tsushimanaka, Kita-ku, Okayama 700-8530, Japan

† Electronic supplementary information (ESI) available. See DOI: 10.1039/d1na00435b

© 2021 The Author(s). Published by the Royal Society of Chemistry

Open Access Article. Published on 10 August 2021. Downloaded on 11/12/2025 2:54:25 PM.
This article is licensed under a Creative Commons Attribution-NonCommercial 3.0 Unported Licence.

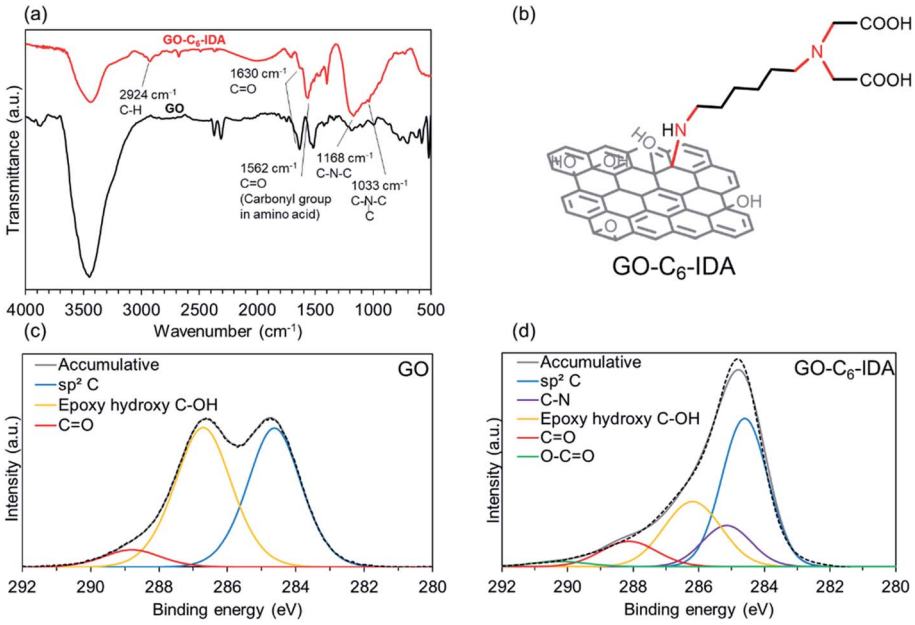

Fig. 1 (a) FT-IR spectra of GO and GO–C_6–IDA, (b) structure of GO–C_6–IDA; XPS analysis of C 1s region of (c) GO, and (d) GO–C_6–IDA.

analysis in this research. Using hexylamine as a model compound, reaction conditions, such as temperature, GO/amine ratio, and pH, were optimized to introduce as many IDA moieties as possible; treatment at 80 °C using a GO/amine ratio of 1 : 1 at pH 9 was found to be the optimum (Tables S2–S4†). Next, a GO–IDA composite with a six-carbon alkyl linker (GO–C_6–IDA) was prepared using the optimum conditions, and structural analyses were performed. For comparison, analyses were also performed for GO heated at 80 °C. FT-IR spectra of GO exhibited peaks at 3450, 1633, 1182, and 1091 cm^{-1}, corresponding to stretching of hydroxyl, carbonyl, epoxy, and carboxy groups, respectively (Fig. 1a). In GO–C_6–IDA, additional peaks were observed, such as a C–H stretching vibration at 2924 cm^{-1}, amino acid-derived C=O band at 1562 cm^{-1}, secondary amine C–N stretching vibration at 1168 cm^{-1}, and tertiary amine at 1033 cm^{-1}.[40,41] These results suggest that GO–C_6–IDA contains the amino acid structure and alkyl linker, consistent with the formation of the desired structure, as shown in Scheme 1. N 1s XPS spectra of GO–C_6–IDA were deconvoluted to peaks at 397.9 eV (5%), 399.3 eV (58%) and 400.9 eV (38%), which were assigned to primary amines, secondary amines and tertiary amines, respectively (Fig. S1†).[42] XPS analysis of the C 1s regions provided information on the structural changes of GO before and after the functionalization. Pristine GO has three main peaks centered at 284.6, 286.7, and 288.8 eV, corresponding to C–C/C=C, C–O, and C=O (Fig. 1c). In GO–C_6–IDA, the C–O peak decreased by half (from 48% to 26%) compared to that in the pristine GO. The deconvolution revealed that an additional peak at 284.5 eV appeared in GO–C_6–IDA, which would be derived from C–N bonds formed by the functionalization (Fig. 1d).[43] This result suggests that the epoxy group on GO reacted *via* ring-opening amination. The introduction of one C_6–IDA moiety on GO by amination through epoxy ring-opening reaction provides five C–N bonds (red lines in Fig. 1b). Since the C–N bond content in GO–C_6–IDA occupies 14% of the total bonds, the proportion of C–N covalent bond to GO can be calculated as 2.3% (see ESI†). This value is much smaller than the decrease of C–O bonds determined by XPS (from 43% to 26%, Fig. 1c and d), suggesting the removal of C–O bonds during the functionalization by the partial reduction of GO.[44] In addition, we compared XRD patterns, Raman spectroscopy, and SEM images of GO and GO–C_6–IDA. From the XRD patterns (Fig. S3†), it was confirmed that GO–C_6–IDA has a broader and partially shifted pattern than GO. This result suggests GO is partially grafted. Raman spectroscopy of GO–C_6–IDA showed the increase of D band (Fig. S4†). This means that the GO was partially reduced during the attachment of IDA moiety.[45] We also compared the SEM images of GO and GO–C_6–IDA (Fig. S5†). GO–C_6–IDA has a smaller size of 1 μm with agglomerated morphology. The surface areas of GO and GO–C_6–IDA by BET were significantly low (*ca.* 10 m^2 g^{-1}) compared with ideal graphene (2630 m^2 g^{-1}),[46] because both materials are strongly

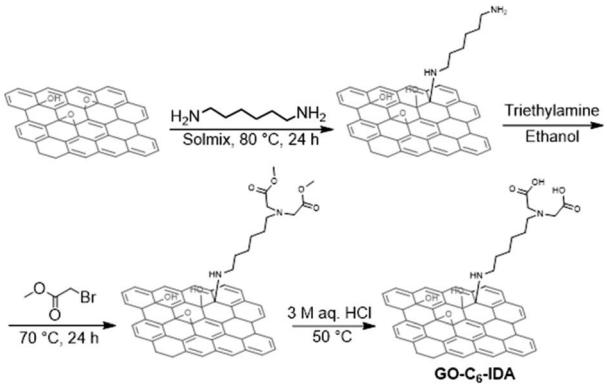

Scheme 1 Preparation of GO–C_6–IDA.

 © 2021 The Author(s). Published by the Royal Society of Chemistry

Open Access Article. Published on 10 August 2021. Downloaded on 11/12/2025 2:54:25 PM.
This article is licensed under a Creative Commons Attribution-NonCommercial 3.0 Unported Licence.

Table 1 CHN elemental analyses of GO and GO–C_6–IDA

Element	Content (wt%) GO	GO–C_6–IDA
C	50	60
H	1.7	4.4
N	0.0	5.2
(O)	48	31

stacked in a dry state. In this study, the available surface of the materials in water is important. Therefore, the surface area in water was measured by methylene blue adsorption method. Methylene blue was adsorbed on GO and GO–C_6–IDA in water, and the amount of adsorption was calculated by UV-vis. Based on a previous study (1 mg of methylene blue on carbon materials corresponds to a surface area of 2.54 m^2),[47] the surface areas of GO and GO–C_6–IDA in water were 432.7 and 592.4 m^2 g^{-1}, respectively.

CHN elemental analyses of GO and GO–C_6–IDA are shown in Table 1. Nitrogen content of GO–C_6–IDA increased by 5.2%, suggesting the introduction of IDA onto GO. Considering the composition of the C_6–IDA moiety ($C_{10}H_{20}N_2O_4$) and the increase of the nitrogen content, GO–C_6–IDA contains 34.5 wt% of the C_6–IDA moiety.

2.2 Metal adsorption tests

Selectivity in metal-ion adsorption was evaluated using a standard solution containing 10 kinds of metal ions (Al, As, B, Cd, Cr, Cu, Mn, Pb, Se, Zn). Initially, the adsorption performance of the IDA molecule and of GO was examined. We found that the IDA molecule has a strong interaction with Cu, and GO has a strong affinity for Pb (Fig. S6†).

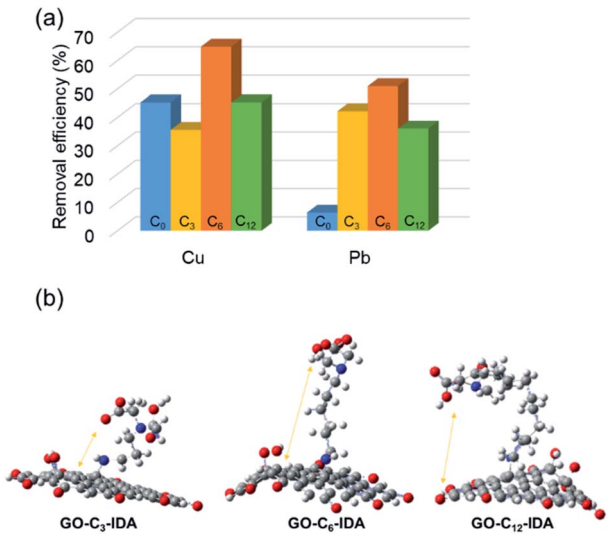

Fig. 2 (a) Cu and Pb adsorption by GO–C_x–IDA. (b) Optimized structures of GO–C_3–IDA, GO–C_6–IDA and GO–C_{12}–IDA by DFT calculation (grey: carbon, blue: nitrogen, red: oxygen, hydrogen is omitted for simplicity).

Based on this result, we investigated metal-ion adsorption using GO–C_x–IDA. The different lengths of alkyl linker may provide different behaviors in water, affecting metal adsorption. The metal adsorption efficiency of Cu was in the order: $C_6 > C_{12} > C_3$ (Fig. 2a). When the alkyl linker was short (C_3), GO–C_x–IDA showed high selectivity for Pb, suggesting GO was mainly responsible for the adsorption by this sample.[48] This result suggests that the IDA in GO–C_6–IDA has a stronger effect than seen in GO–C_3–IDA. We assume that the IDA moieties interact with the GO surface when the alkyl linker is short, and lose their chelating effect for metal ions. In contrast, a longer hydrophobic alkyl linker prevents IDA from interacting with the GO surface, enabling the IDA to chelate metal ions instead. This assumption was confirmed by DFT calculations of optimized structures; in GO–C_3–IDA, the IDA moiety is closer to the GO surface than it is in GO–C_6–IDA (Fig. 2b). In addition, calculation of the chelation energy[49] between IDA and Cu revealed that the alkyl substituent enhanced the stabilization (Table S6†). However, when the alkyl linker was longer (*e.g.*, C_{12}), its hydrophobicity restricted the covalent functionalization reaction, limiting the introduction of the IDA moiety, and reducing adsorption performance (Table S7†).

Next, the adsorption experiment was carried out at pH 1 (the as-obtained metal standard solution) and pH 7 (adjusted with aq. NaOH). The experiment cannot be performed under alkaline conditions, because of the formation of metal hydroxide precipitates. At pH 7, improved selectivity and efficiency were observed for all metal ions compared with those at pH 1. This would be because the surface charge of GO becomes positive under acidic conditions, and repulsion of metal ions occurs.[50] Furthermore, coordinating and chelating functional groups on GO–C_6–IDA in acidic solutions are COOH and OH; thus, the decrease in pH inhibits coordination and chelation. In contrast, in neutral to alkaline conditions, carboxylate and alkoxylate are generated, and the surface of GO is negatively charged, leading to the improved interaction with metal ions. At pH 7, GO–C_6–IDA showed the following order of adsorption: Cu > Pb > As > B > Zn > Al ≈ Se > Cr ≈ Cd (Fig. 3). This result does not follow the order for the stability constants of the corresponding IDA complexes for metal ions: Cu > B > Cr > Cd ≈ Pb (Fig. S6†),[51,52]

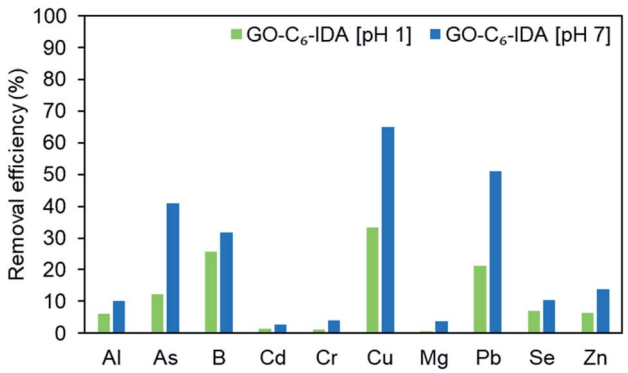

Fig. 3 The removal efficiency of 10 different metal ions using GO–C_6–IDA at pH 1 and 7.

Open Access Article. Published on 10 August 2021. Downloaded on 11/12/2025 2:54:25 PM.
This article is licensed under a Creative Commons Attribution-NonCommercial 3.0 Unported Licence.

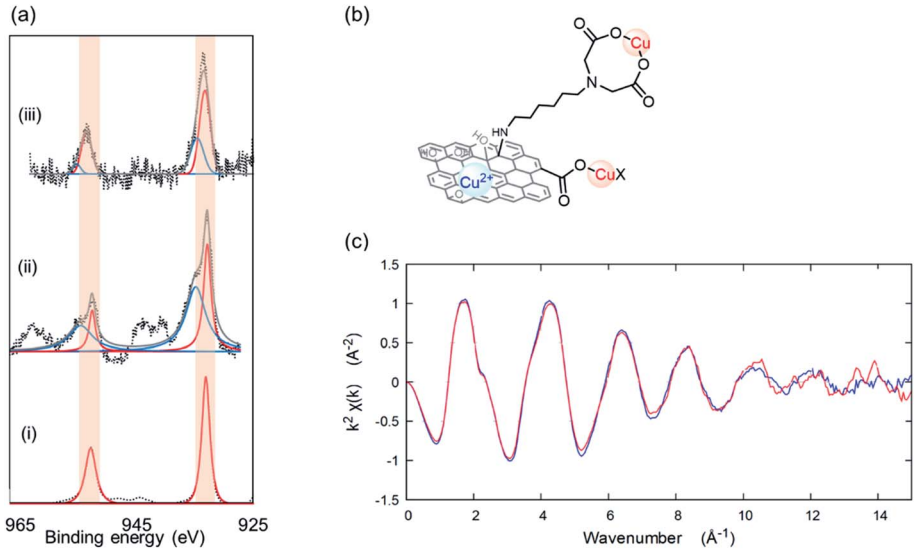

Fig. 4 (a) XPS analysis of the Cu 2p region for (i) $Cu(OAc)_2$, (ii) Cu@GO, and (iii) Cu@GO–C_6–IDA. Red lines correspond to Cu carboxylate, and blue lines correspond to Cu^{2+} ion. (b) Proposed adsorption modes of Cu on GO–C6–IDA. (c) EXAFS spectra of Cu@IDA (red line) and Cu@GO–C6–IDA (blue line) at *k* space.

suggesting a synergetic effect of GO, alkyl linker, and IDA. The utilization ratio of the IDA moiety of GO–C_6–IDA for Cu was calculated to be 97% (Table S9†).

2.3 Fine structure analysis of metal-adsorbed GO–C_6–IDA

To understand metal-ion selectivity of GO–C_6–IDA, detailed structural analyses were performed. XPS analysis of Cu-adsorbed GO (Cu@GO) and GO–C_6–IDA (Cu@GO–C_6–IDA) showed a different chemical state compared with that seen in the Cu precursor, $CuSO_4 \cdot 5H_2O$ (Fig. S10†). Assuming that the Cu ion coordinates to the carboxyl group, $Cu(OAc)_2$, as a reference Cu carboxylate compound, was analyzed by XPS (Fig. 4a and i). Deconvolution of the Cu $2p_{3/2}$ region of Cu@GO and Cu@GO–C_6–IDA revealed that both materials have peaks at 953 and 933 eV (red lines in Fig. 4a), which correspond to the lines found for $Cu(OAc)_2$. Other peaks at 955 and 935 eV are assigned to Cu ion derived from $Cu(OH)_2$ (blue lines in Fig. 4a); Cu@GO contained a larger amount of Cu ion on its surface.[53] Cu@GO–C_6–IDA contained 73% of Cu carboxylate and 27% of Cu ion, while Cu@GO contained 37% of Cu carboxylate and 63% of Cu ion. These results confirm the contribution of IDA moiety to the Cu adsorption (Fig. 4b). For a more detailed understanding of the interaction between Cu and GO–C_6–IDA, we measured X-ray absorption fine structure (XAFS). XAFS analysis is further categorized as either X-ray absorption near edge structure (XANES, −50 to +50 eV) or extended X-ray absorption fine structure (EXAFS, +50 to +1500 eV). XANES provides information on the electronic states and coordination structures of an element.[54] We found that Cu in Cu@GO–C_6–IDA was in a divalent or higher state (Fig. S11†). EXAFS provides information on the local structure (number of coordinated atoms, interatomic distance, and coordinated atomic species) around the target element.[55] Comparison of the EXAFS vibrations of Cu–IDA complex[56,57] and Cu@GO–C_6–IDA revealed that both materials showed similar patterns (Fig. 4c), suggesting the successful coordination of Cu by the IDA moiety. Finally, the Pb chemical state was determined for Pb@GO–C_6–IDA, because Pb is proposed to adsorb onto the GO surface.[58] XPS analyses of the Pb $4f_{7/2}$ region for Pb–IDA complex, Pb@GO, and Pb@GO–C_6–IDA were performed. The chemical state (as indicated by the XPS spectra) of Pb in Pb@GO–C_6–IDA was different from that in the Pb–IDA complex, but similar to that of Pb@GO (Fig. S12†), confirming the adsorption of Pb directly onto the GO surface (Fig. S13†).

3. Conclusions

In conclusion, we have synthesized GO–C_x–IDA with different lengths of alkyl chain linkers. C_6 chain linker was the optimum for metal adsorption. GO–C_6–IDA showed selective adsorption for Cu because of the chelating interaction between the Cu and the IDA moiety. GO is known to have a strong affinity with Pb, but IDA functionalization altered the metal-ion selectivity. The modes of adsorption of Cu and Pb on GO–C_6–IDA were analyzed by EXAFS and XPS. This study enables us to construct a strategy for selective adsorption of specific metals by functionalization with specific chelating moieties, and choice of appropriate linkers and surface chemistry of GO.

4. Experimental

4.1 Materials

Graphite was purchased from Bay Carbon Inc.; 1,3-propanediamine, 1,6-hexanediamine, 60% H_3AsO_4 and $Pb(OAc)_4$ were purchased from Tokyo Chemical Industry Co., Ltd; and 1,12-dodecanediamine, methyl 2-bromoacetate, $CuSO_4 \cdot 5H_2O$, methylene blue and NaOH were purchased from Fujifilm Wako Pure Chemical Industries, Ltd. Triethylamine, HCl, and HNO_3 were

 © 2021 The Author(s). Published by the Royal Society of Chemistry

Open Access Article. Published on 10 August 2021. Downloaded on 11/12/2025 2:54:25 PM.
This article is licensed under a Creative Commons Attribution-NonCommercial 3.0 Unported Licence.

purchased from Nacalai Tesque Co., Ltd; iminodiacetic acid (IDA) and metal standard solution V (100 mg L^{-1} Al, As, B, Cd, Cr, Cu, Mn, Pb, Se, Zn in 0.1 mol L^{-1} HNO_3 aq.) were purchased from Kanto Chemical Co., Ltd; and solmix (ethanol: 85.5%, *n*-propyl alcohol: 9.6%, methanol: 4.9%, water: less than 0.2%) was purchased from Japan Alcohol Trading Co., Ltd. The synthesized materials were characterized by Fourier transform infrared (FT-IR) spectroscopy (Shimadzu, IR Tracer 100), X-ray photoelectron spectroscopy (XPS) (JEOL, JPS-9030), X-ray diffraction (XRD) (Malvern Panalytical, Aeris), Scanning Electron Microscope (SEM) (Hitachi High-Tech Science Corporation, S-5200), Raman spectroscopy (JASCO Corporation, NRS-3100) and CHN elemental analysis (EA) (PerkinElmer, 2400II). The metal-ion concentrations were measure by inductively coupled plasma atomic emission spectroscopy (ICP-AES) (Seiko Instruments, VISTA-PRO). Cu K edge X-ray absorption fine structure (XAFS) spectra were acquired in the BL01B1 beamline at Spring-8. Transmission spectra were obtained using a double-crystal Si(111) monochromator. The energy calibration was accomplished by adjusting the first peak top of the spectrum of Cu foil to 8980.3 eV. The oxygen content was calculated from EA, as shown in eqn (1).

$$O(wt\%) = 100 - (C + H + N) \quad (1)$$

4.2 Synthesis of graphene oxide–iminodiacetic acid composite (GO–C_x–IDA)

GO was prepared by the modified Hummers' method.[59] 33 g of graphite and 990 mL of sulfuric acid were mixed and stirred while cooling with ice water. Next, 99 g of potassium permanganate was slowly added, and the mixture was allowed to stand at 35 °C for 2 hours. 990 mL of ice water was then added, after which 30% hydrogen peroxide solution was gradually added to the obtained reaction mixture at room temperature until foaming did not occur. After that, the mixture was stirred for 30 minutes. Centrifugation was repeated until pH >3. For the preparation of GO–C_6–IDA (Scheme 1), 0.25 g of 1,6-diaminohexane (2.2 mmol) was added to 20 g of GO dispersion (1.24 wt% in water) using 30 mL of solmix as a solvent, and the mixture was stirred at 80 °C for 24 hours. The reaction mixture was centrifuged twice with water. Afterwards, 0.32 mL of triethylamine (2.3 mmol) was added to the diaminohexane-treated GO using 30 mL of ethanol as a solvent. 0.23 mL of methyl-2-bromoacetate (2.4 mmol) was added, and the mixture was stirred at 70 °C for 24 hours.[60] The reaction mixture was centrifuged twice with water: solmix = 1 : 1, once with 3 M aq. HCl, and twice with water. The GO–C_6–IDA was obtained as a powder by freeze-drying overnight. Other GO–IDA composites, such as GO–C_3–IDA and GO–C_{12}–IDA were prepared with the same procedure using 1,3-diaminopropane and 1,12-diaminododecane, respectively. GO–C_0–IDA was prepared by mixing GO and IDA, and the reaction mixture was centrifuged twice with water: solmix = 1 : 1, once with 3 M aq. HCl, and twice with water.

4.3 Metal adsorption test

10 mg of GO–C_x–IDA and 2 mL of test solution containing 10 mg L^{-1} of Al, As, B, Cd, Cr, Cu, Mn, Pb, Se, and Zn in 0.01 mol L^{-1} aq. HNO_3 were stirred for 0.5 h, and homogenized with an ultrasonic homogenizer (BILON, BILON150-Y) for 10 minutes. The mixture was suction-filtered using a membrane filter (isopore 0.2 μm hydrophilic membrane) and washed with MilliQ water. The obtained solution is termed Sample 1. To double-check the amount of adsorbed metal ions on GO–IDA, the membrane with GO–IDA was immersed in 5 mL of 2 M HNO_3 to leach out the metal ions,[61] dispersed by sonication for 4 minutes, stirred for 1 h, and suction-filtered using another membrane filter. The obtained solution was termed Sample 2 (Scheme 2). The metal-ion concentrations of Sample 1 and Sample 2 were measured by ICP-AES. The initial metal concentration is denoted C_i, the metal-ion concentration of Sample 1 is C_w (metal ions in water), and of Sample 2 is C_a (metal ions adsorbed on GO–IDA). The removal efficiency was calculated from eqn (2) and (3).[48]

Scheme 2 Adsorption/desorption process of metal ions on/from GO–C_6–IDA.

$$\text{Removal efficiency } (\%) = C_a/C_i \quad (2)$$

$$C_i = C_w + C_a \quad (3)$$

Author contributions

R. S. synthesized materials, analyzed their structure, and evaluated their performance. K. K. performed structural analysis. Y. N. conceived the project and designed the experiments. All authors have given approval to the final version of the manuscript.

Conflicts of interest

There are no conflicts to declare.

Acknowledgements

We are grateful to Dr Seiji Obata, Dr Hideaki Nagare, and Mr Koichiro Kubo for their help with the instrumentation facilities. The XAFS measurements were performed in SPring-8 (Proposal No. 2020A1254). This research was supported by JSPS KAKENHI (20H05224) and JST CREST (JPMJCR18R3).

Notes and references

1 Z. Li, Z. Ma, T. J. van der Kuijp, Z. Yuan and L. Huang, *Sci. Total Environ.*, 2014, **468–469**, 843–853.
2 S. S. Ahluwalia and D. Goyal, *Bioresour. Technol.*, 2007, **98**, 2243–2257.

Open Access Article. Published on 10 August 2021. Downloaded on 11/12/2025 2:54:25 PM.
This article is licensed under a Creative Commons Attribution-NonCommercial 3.0 Unported Licence.

3 V. Masindi and K. L. Muedi, *Environment Contamination by Heavy Metals*, ed. HosamEl-Din M. S. and F. A. Refaat, IntechOpen, London, UK, 2018.
4 P. Wongsasuluk, S. Chotpantarat, W. Siriwong and M. Robson, *Environ. Geochem. Health*, 2014, **36**, 169–182.
5 S. Muhammad, M. T. Shah and S. Khan, *Microchem. J.*, 2011, **98**, 334–343.
6 B. K. Mandal and K. T. Suzuki, *Talanta*, 2002, **58**, 201–235.
7 C. K. Jain and I. Ali, *Water Res.*, 2000, **34**, 4304–4312.
8 J. L. Barringer, Z. Szabo and P. A. Reilly, Occurrence and mobility of mercury in groundwater, *Current Perspectives in Contaminant Hydrology and Water Resources Sustainability*, IntechOpen, 2013, ch, n.d., 5, pp. 118–150.
9 A. Kubier, K. Hamer and T. Pichler, *Integr. Environ. Assess. Manage.*, 2020, **16**, 103–113.
10 Y. Sang, Q. Gu, T. Sun, F. Li and C. Liang, *J. Hazard. Mater.*, 2008, **153**, 860–866.
11 B. K. Mandal, T. R. Chowdhury, G. Samanta, G. K. Basu, P. P. Chowdhury, C. R. Chanda, D. Lodh, N. K. Karan, R. K. Dhar, D. K. Tamili, D. Das, K. C. Saha and D. Chakraborti, *Curr. Sci.*, 1996, **70**, 976–986.
12 S. A. Cavaco, S. Fernandes, M. M. Quina and L. M. Ferreira, *J. Hazard. Mater.*, 2007, **144**, 634–638.
13 C. E. R. Barquilha, E. S. Cossich, C. R. G. Tavares and E. A. da Silva, *J. Water Process. Eng.*, 2019, **32**, 100904.
14 Y. Benito and M. L. Ruíz, *Desalination*, 2002, **142**, 229–234.
15 I. Ali, T. A. Khan and M. Asim, *Sep. Purif. Rev.*, 2011, **40**, 25–42.
16 O. Tavakoli, V. Goodarzi, M. R. Saeb, N. M. Mahmoodi and R. Borja, *J. Hazard. Mater.*, 2017, **334**, 256–266.
17 A. F. Shaaban, D. A. Fadel, A. A. Mahmoud, M. A. Elkomy and S. M. Elbahy, *J. Environ. Chem. Eng.*, 2014, **2**, 632–641.
18 Y.-H. Li, J. Ding, Z. Luan, Z. Di, Y. Zhu, C. Xu, D. Wu and B. Wei, *Carbon*, 2003, **41**, 2787–2792.
19 F. S. Awad, K. M. AbouZeid, W. M. A. El-Maaty, A. M. El-Wakil and M. S. El-Shall, *ACS Appl. Mater. Interfaces*, 2017, **9**, 34230–34242.
20 A. Azimi, A. Azari, M. Rezakazemi and M. Ansarpour, *ChemBioEng Rev.*, 2017, **4**, 37–59.
21 J.-G. Mao and A. Clearfield, *Inorg. Chem.*, 2002, **41**, 2319–2324.
22 Ö. Szabadka, *Talanta*, 1982, **29**, 183–187.
23 D. Muraviev, A. Gonzalo and M. Valiente, *Anal. Chem.*, 1995, **67**, 3028–3035.
24 A. Efligenir, M. A. Mohamed, P. Fievet and N. Fatin-Rouge, *J. Environ. Chem. Eng.*, 2013, **1**, 448–452.
25 P. Sun, M. Zhu, K. Wang, M. Zhong, J. Wei, D. Wu, Z. Xu and H. Zhu, *ACS Nano*, 2013, **7**, 428–437.
26 R. K. Joshi, P. Carbone, F. C. Wang, V. G. Kravets, Y. Su, I. V. Grigorieva, H. A. Wu, A. K. Geim and R. R. Nair, *Science*, 2014, **343**, 752–754.
27 H. Huang, Y. Mao, Y. Ying, Y. Liu, L. Sun and X. Peng, *Chem. Commun.*, 2013, **49**, 5963–5965.
28 Y. Han, Z. Xu and C. Gao, *Adv. Funct. Mater.*, 2013, **23**, 3693–3700.
29 M. Elimelech and W. A. Phillip, *Science*, 2011, **333**, 712–717.
30 M. Hu and B. Mi, *Environ. Sci. Technol.*, 2013, **47**(8), 3715–3723.
31 R. Sitko, E. Turek, B. Zawisza, E. Malicka, E. Talik, J. Heimann, A. Gagor, B. Feist and R. Wrzalik, *Dalton Trans.*, 2013, **42**, 5682–5689.
32 H. Wang, X. Yuan, Y. Wu, H. Huang, G. Zeng, Y. Liu, X. Wang, N. Lin and Y. Qi, *Appl. Surf. Sci.*, 2013, **279**, 432–440.
33 S.-T. Yang, Y. Chang, H. Wang, G. Liu, S. Chen, Y. Wang, Y. Liu and A. Cao, *J. Colloid Interface Sci.*, 2010, **351**, 122–127.
34 V. Chandra, J. Park, Y. Chun, J. W. Lee, I.-C. Hwang and K. S. Kim, *ACS Nano*, 2010, **4**, 3979–3986.
35 C. J. Madadrang, H. Y. Kim, G. Gao, N. Wang, J. Zhu, H. Feng, M. Gorring, M. L. Kasner and S. Hou, *ACS Appl. Mater. Interfaces*, 2012, **4**, 1186–1193.
36 S. Luo, X. Xu, G. Zhou, C. Liu, Y. Tang and Y. Liu, *J. Hazard. Mater.*, 2014, **274**, 145–155.
37 L. Cui, Y. Wang, L. Gao, L. Hu, L. Yan, Q. Wei and B. Du, *Chem. Eng. J.*, 2015, **281**, 1–10.
38 A. Abu-Nada, G. McKay and A. Abdala, *Nanomaterials*, 2020, **10**, 595.
39 N. D. Q. Chau, G. Reina, J. Raya, I. A. Vacchi, C. Ménard-Moyon, Y. Nishina and A. Bianco, *Carbon*, 2017, **122**, 643–652.
40 J. Zhang, H. Yang, G. Shen, P. Cheng, J. Zhang and S. Guo, *Chem. Commun.*, 2010, **46**, 1112–1114.
41 N. Morimoto, T. Kubo and Y. Nishina, *Sci. Rep.*, 2016, **6**, 21715.
42 M.-C. Hsiao, S.-H. Liao, Y.-F. Lin, C.-A. Wang, N.-W. Pu, H.-M. Tsai and C.-C. M. Ma, *Nanoscale*, 2011, **3**, 1516–1522.
43 F. T. Johra and W.-G. Jung, *Appl. Surf. Sci.*, 2015, **357**, 1911–1914.
44 M. Hada, K. Miyata, S. Ohmura, Y. Arashida, K. Ichiyanagi, I. Katayama, T. Suzuki, W. Chen, S. Mizote, T. Sawa, T. Yokoya, T. Seki, J. Matsuo, T. Tokunaga, C. Itoh, K. Tsuruta, R. Fukaya, S. Nozawa, S. Adachi, J. Takeda, K. Onda, S. Koshihara, Y. Hayashi and Y. Nishina, *ACS Nano*, 2019, **13**, 10103–10112.
45 Y. Nishina and S. Eigler, *Nanoscale*, 2020, **12**, 12731–12740.
46 S. Stankovich, D. A. Dikin, G. H. B. Dommett, K. M. Kohlhaas, E. J. Zimney, E. A. Stach, R. D. Piner, S. T. Nguyen and R. S. Ruof, *Nature*, 2006, **442**, 282–286.
47 M. J. McAllister, J.-L. Li, D. H. Adamson, H. C. Schniepp, A. A. Abdala, J. Liu, M. Herrera-Alonso, D. L. Milius, R. Car, R. K. Prud'homme and I. A. Aksay, *Chem. Mater.*, 2007, **19**, 4396–4404.
48 R. Sitko, E. Turek, B. Zawisza, E. Malicka, E. Talik, J. Heimann, A. Gagor, B. Feist and R. Wrzalik, *Dalton Trans.*, 2013, **42**, 5682–5689.
49 A. Parameswari, S. Hussain, R. Premkumar, R. M. Asath and A. M. F. Benial, *Anal. Chem. Lett.*, 2018, **8**, 437–456.
50 B. Konkena and S. Vasudevan, *J. Phys. Chem. Lett.*, 2012, **3**, 867–872.
51 S. Chaberek and A. E. Martell, *J. Am. Chem. Soc.*, 1952, **74**, 5052–5056.
52 S. Chaberek, R. C. Courtney and A. E. Martell, *J. Am. Chem. Soc.*, 1952, **74**, 5057–5060.

 © 2021 The Author(s). Published by the Royal Society of Chemistry

Open Access Article. Published on 10 August 2021. Downloaded on 11/12/2025 2:54:25 PM.
This article is licensed under a Creative Commons Attribution-NonCommercial 3.0 Unported Licence.

53 D. W. Shoesmith, S. Sunder, M. G. Bailey, G. J. Wallace and F. W. Stanchell, *J. Electroanal. Chem. Interfacial Electrochem.*, 1983, **143**, 153–165.
54 F. Farges and G. E. Brown, *Geochim. Cosmochim. Acta*, 1997, **61**, 1863–1870.
55 T. Fujikawa, *Nippon Kessho Gakkaishi*, 1985, **27**, 357–373.
56 M. J. Lawless, S. Ghosh, T. F. Cunningham, A. Shimshi and S. Saxena, *Phys. Chem. Chem. Phys.*, 2017, **19**, 20959–20967.
57 I. Moreno-Villoslada, F. González, M. Jofré, P. Chandía, S. Hess and B. L. Rivas, *Macromol. Chem. Phys.*, 2005, **206**, 1541–1548.
58 S. Park, K. S. Lee, G. Bozoklu, W. Cai, S. T. Nguyen and R. S. Ruoff, *ACS Nano*, 2008, **2**(3), 572–578.
59 W. S. Hummers and R. E. Offeman, *J. Am. Chem. Soc.*, 1958, **80**, 1339.
60 R. Schibli, R. Schwarzbach, R. Alberto, K. Ortner, H. Schmalle, C. Dumas, A. Egli and P. A. Schubiger, *Bioconjugate Chem.*, 2002, **13**, 750–756.
61 M. A. Habila, Z. A. ALOthman, A. M. El-Toni, S. A. Al-Tamrah, M. Soylak and J. P. Labis, *Microchim. Acta*, 2017, **184**, 2645–2651.